Magnetic scanning and interpretation of paleomagnetic data from Prague Synform's volcanics

GUNTHER KLETETSCHKA[1,2], PETR SCHNABL[1], KRISTÝNA ŠIFNEROVÁ[1], ZUZANA TASÁRYOVÁ[2], ŠTĚPÁN MANDA[2] AND PETR PRUNER[1]

1 Institute of Geology, Academy of Sciences of the Czech Republic, v.v.i., Rozvojová 269, Praha 6, Czech Republic (kletetschka@gmail.com)

2 Charles University in Prague, Faculty of Science, Albertov 6, 128 43 Praha 2, Czech Republic

Received: March 22, 2012; Revised: June 7, 2012; Accepted: June 15, 2012

ABSTRACT

Magnetic images have been produced at the distance of 0.1 mm from the polished basaltic thin sections of rocks from Prague Synform in Barrandian area. Three different magnetic textures were seen and when combined with optical imaging could be related to petrological features. The first magnetic texture revealed that most of the magnetic signature is localized within the amygdales formed later after the basalts became part of the sedimentary sequence. The second texture showed that the basaltic body contains large grain size distribution of magnetic carriers possibly with variable viscous magnetizations. The third texture suggested a presence of magnetic anisotropy of igneous origin. Such textural magnetic information along with the paleomagnetic characteristics of the basaltic rocks of Silurian age constrained the overall geological interpretation.

Keywords: paleomagnetism, magnetic scanner, magnetic mineralogy, amygdales, magnetic anomalies, magnetic texture, Barrandian

1. INTRODUCTION

Magnetic anomalies were obtained remotely from the surface of Mars and their interpretation is often quite complicated (*Weiss et al., 2000*; *Kletetschka et al., 2000a,b, 2004*; *Connerney et al., 2001, 2005*). However, magnetic anomalies on Earth have complication of being generated not only by magnetic remanence, but also with inducing geomagnetic field (*Kletetschka and Stout, 1998*; *Wasilewski et al., 2002*; *Kletetschka et al., 2006*). Magnetic anomalies on Mars do not contain induced magnetic component (*Kletetschka, 2000*; *Kletetschka et al., 2000b, 2004, 2005, 2009*). In order to understand the geological context of magnetic anomalies similar to those on Mars and with the advance of technological automatic processes (e.g. Superconducting Quantum Interference Device (SQUID) based magnetic microscope (*Oda et al., 2011*)) we have developed a simple magnetic scanner. Our scanner has a magnetic anomaly detection mode similar to the mode of the SQUID microscope used on basalts (*Weiss et al., 2007a*) or magneto-optical imaging mode (*Uehara et al., 2010*). Such magnetic scans contain micro-scale magnetic information and therefore are helping us in the interpretation of

geologic thin sections or polished plugs of rocks that are associated with strong magnetization (hundreds of A/m). Previous studies of this kind were focusing mainly on meteorites due to the generally high density of their magnetic carriers (*Acuna et al., 2002*; *Wasilewski et al., 2002*; *Kletetschka et al., 2003*). Reports from the Prague Synform (*Aifa et al., 2007*) indetify rocks with substantial magnetic properties, allowing magnetic detection with the Hall probe that we combined into a magnetic scan over its surface with resolution of about 0.2 mm. Such resolution allows more detailed information about the nature of the remanent magnetization and its origin.

2. GEOLOGICAL SETTING OF THE SAMPLES

We studied three basaltic samples from the Silurian volcanic region that is located in the NE sector of the today's relict of the Prague Synform. Revival of basaltic volcanism since the Late Ordovician generated a specific geological structure, where olivine basalt magma ascended along several deep, ENE-WSW trending fissures, parallel to the longitudinal axis of the Prague Synform. Additional basaltic fissures went along WNW-ESE trending faults perpendicular to this axis (*Kříž, 1991*).

The volcano-sedimentary sequence (Telychian–Gorstian) is exposed in the Svatý Jan volcanic center in the northern flank of Holyň-Hostim Syncline between the villages of Beroun-Tetín and Mezouň. The syncline is composed of an up to 400 m thick succession of pyroclastics, tuffs, tuffitic shales, shallow water limestones and both effusive basalts and intrusive dikes (*Kříž, 1992, 1998*). Additionally, the central part of Svatý Jan volcanic center formed an emergent elevation above sea level from the early Wenlock to late Llandovery, which is indicated by a presence of sub-aerial volcanic products. Despite the significant thickness of the volcano-sedimentary complex, the effusive basalts formed only minor part of the succession and are concentrated into a few stratigraphic intervals.

The first of the three sites described here is the site C5, near Loděnice-Bubovice road cut (Černidla).This road cut (~210 m) is along the road between the villages of Loděnice and Bubovice revealing a section of volcano-sedimentary facies of the Motol Formation ranging from mid-Sheinwoodian to late-Homerian (Wenlock). The exposed volcano-sedimentary succession (early Sheinwoodian–Gorstian) consists of tuffitic shales and yellow-brown tuffs, with thin beds and lenses of skeletal limestones and mudstones corresponding to shallow-marine deposition, which are interrupted with several thick basalt lava flows (*Bouček, 1942*; *Kříž, 1992*).

The second site, Si07, is from the U Vitáčků Section near Lištice. That section is of Wenlock/Ludlow age and is along the road-cut on the left side of the Berounka river, 2 km east from the Beroun railway station and represents the volcano-sedimentary succession at the boundary between the Motol and Kopanina Formation. There the top of the volcanic complex of the Lištice section (tuffs, hyaloclastites, tuffitic shales) is exposed, overlain by a 4 m thick basalt with calcite amygdales. The sub-marine lava flow is overlain by a succession of grey bioclastic limestones containing brachiopod- and coral-dominated fauna corresponding with "the *C. beaumonti* Horizon", of Gorstian Stage (*Kříž, 1991*). Thus, the underlying volcaniclastic deposits and effusions are likely of the earliest Gorstian age resting on the limestone of latest Wenlock age (Kozla facies). Major exposed rocks consist of agglomerates and yellow-green coarse-grained tuffs, which contain

basaltic bombs and limestone xenoliths. The 4 m thick effusive lava flow forms the top of the volcanic sequence (*Kodym et al., 1931*; *Fišera, 1965a*; *Horný, 1965*; *Kříž, 1992*).

The third site, Si08, comes from the Lištice quarry. The road to this quarry leads from Lištice to Beroun, exposing the basaltic intrusion and calcareous shales of the lowermost Motol Formation, Telychian in age (Llandovery), representing the lowermost part of the Svatý Jan volcano-sedimentary section near Lištice. Exposure in the eastern part of the quarry includes a development of 60 cm thick fine-grained datolite chert representing the contact aureole between basaltic intrusion and calcareous shale. It contains graptolites of the *S. grandis* Subzone, Telychian, latest Llandovery (*P. Štorch, personal communication*, see also *Kodym et al., 1931*). The maximum age of the basaltic intrusion correspond to the latest Llandovery (*Strnad, 1961*; *Fišera, 1965b*).

Paleomagnetically these formentioned units are of bimodal age with poles separated by large offset giving Ordovician and Permocarboniferous ages (*Krs et al., 2001*).

3. MATERIAL AND METHODS

3.1. Sampling

Several oriented cores had been obtained from each of the sites. Each site provided about 12 cores that were used for making a geological thin section and magnetic scanning.

3.2. Scanning Magnetic Microscopy

We used a magnetic scanner built by Youngwood Science and Engineering (YSE), a US company that builds to desired specifications (youngwoodscience@gmail.com). The scanner consists of a stationary hall probe and a 2D motorized stage whose motion is controlled by software (MagScan) also developed by YSE. The hall probe senses the magnetic component perpendicular to the scanning surface (e.g. geological thin section) from a distance of 0.1 mm, and returns its value along with the *X*-*Y* coordinates to the computer. The output is a 2D image that shows the values of magnetization detected over the surface of the sample. For all of our images the scanned area is 17×17 mm (the maximum capability of the 2D stage) with a spatial step of 0.2 mm between and along the scan lines.

We scanned three thin sections that were cut from three basaltic cores of the Barrandian area. These sections were scanned in magnetically saturated state both with and without any magnetic shielding. We found no significant difference, detecting mostly saturation remanence, and data in Figs 1–3 were obtained without any magnetic shielding. Saturation remanence in 3 T pulse field was acquired from top to bottom of the images in Figs 1–3.

3.3. Remanent Magnetization

Paleomagnetic directions were obtained from from cores 2.5 cm in diameter that were drilled out from the volcanic units so that their orientation was preserved in spatial coordinates. After measurements of natural remanent magnetization (*NRM*), these samples were subject of progressive thermal and/or alternating magnetic field (AF) demagnetizations. Thermal demagnetization was achieved using the MAVACS (Magnetic Vacuum Control System (*Příhoda et al., 1989*) equipment with temperatures ranging

between 80°C and 580°C and with step intervals between 30°C and 40°C (see the steps in Figs 5 and 6 later). Demagnetization by AF (LDA-3 apparatus, AGICO Brno) up to 100 mT was done with the steps of every 5–20 mT. NRM measurements were carried out using either the spinner magnetometers JR-5A or JR-6A (AGICO Brno). The magnetic susceptibility (k) of the specimens was determined using a KLY-4 Kappabridge (*Jelínek, 1966, 1973*) by AGICO Brno. Results of measurements were analyzed using the software package Remasoft (*Chadima and Hrouda, 2006*). Multicomponent analysis separated the remanent magnetization components (*Kirschvink, 1980*; *Man, 2003*).

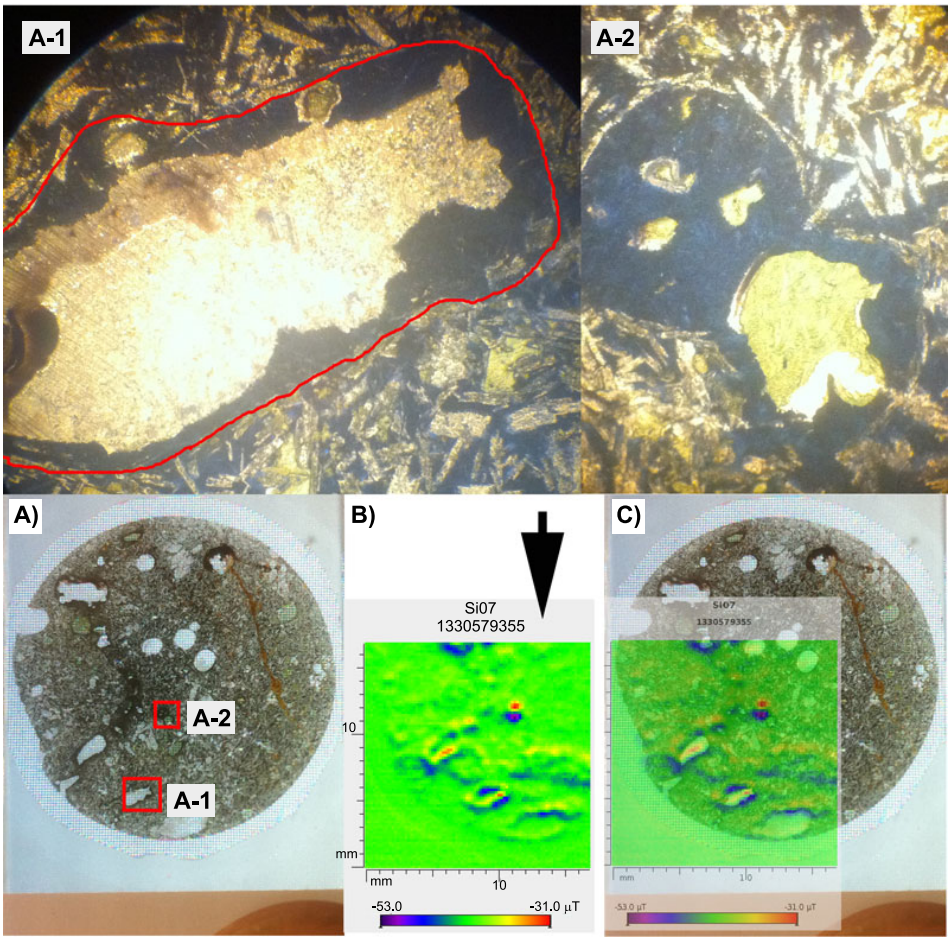

Fig. 1. Combination of the optical plain polarized transparent image with the magnetic scan. **A)** Optical image of the thin section Si07. Red rectangles are insets A-1 and A-2. **B)** Magnetic scan of the thin section from Si07 pulse magnetized by 3 T along the black arrow. **C)** Overlap of the magnetic and optical images.

At each step of the thermal demagnetization, the bulk magnetic susceptibility value was checked. Thermal treatment often results in chemical changes involving the magnetic carriers and thus compromising the data. Chemical changes often result in increase or decrease of the amount of magnetic carriers in the sample and therefore magnetic susceptibility conveniently monitors any chemical changes in the sample.

3.4. Coercivity Spectra

After AF demagnetization the samples were progressively magnetized by pulse magnetizer (MMPM10, Magnetic Measurements, U.K.) until they reached the saturation and then stepwise demagnetized by AF using LDA-3, until its maximum obtainable AF field of 100 mT (for the specific steps see Fig. 4).

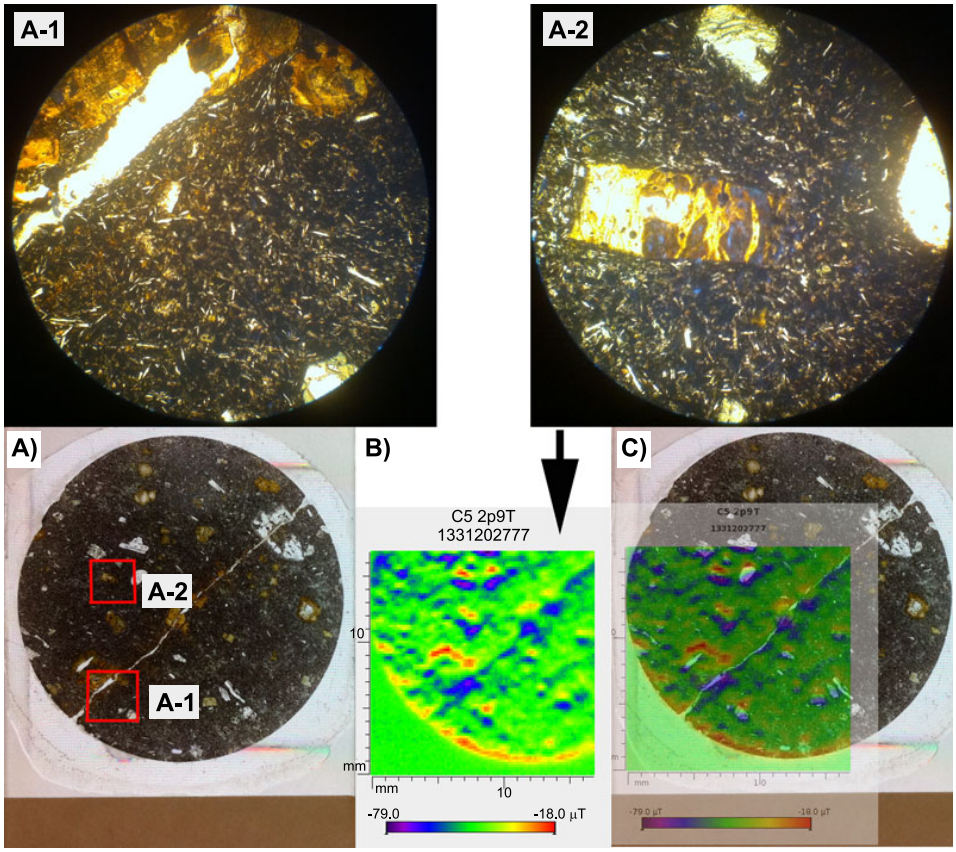

Fig. 2. Combination of the optical transparent image with the magnetic scan. **A)** Optical image of the thin section C5. Two red rectangles are locations of the two insets, A-1, and A-2. **B)** Magnetic scan of the thin section C5 pulse magnetized by 3 T along the black arrow. **C)** Overlap of the magnetic and optical images.

3.5. Microscopy

Standard geological thin sections were obtained from the relevant samples C5 (Černidla), Si07 (Lištice roadcut), and Si08 (Lištice quarry). Because the magnetic scanning has a special resolution of only 0.2 mm and we needed comparison at the similar scale we placed the standard thin sections on a light table and took a photograph that was subsequently combined with the magnetic scan images (Figs 1–3). The detailed nature of the regions with magnetic anomalies detected by the scanner was imaged and photographed using a polarized light optical microscope Spencer at magnification of 62.5 times.

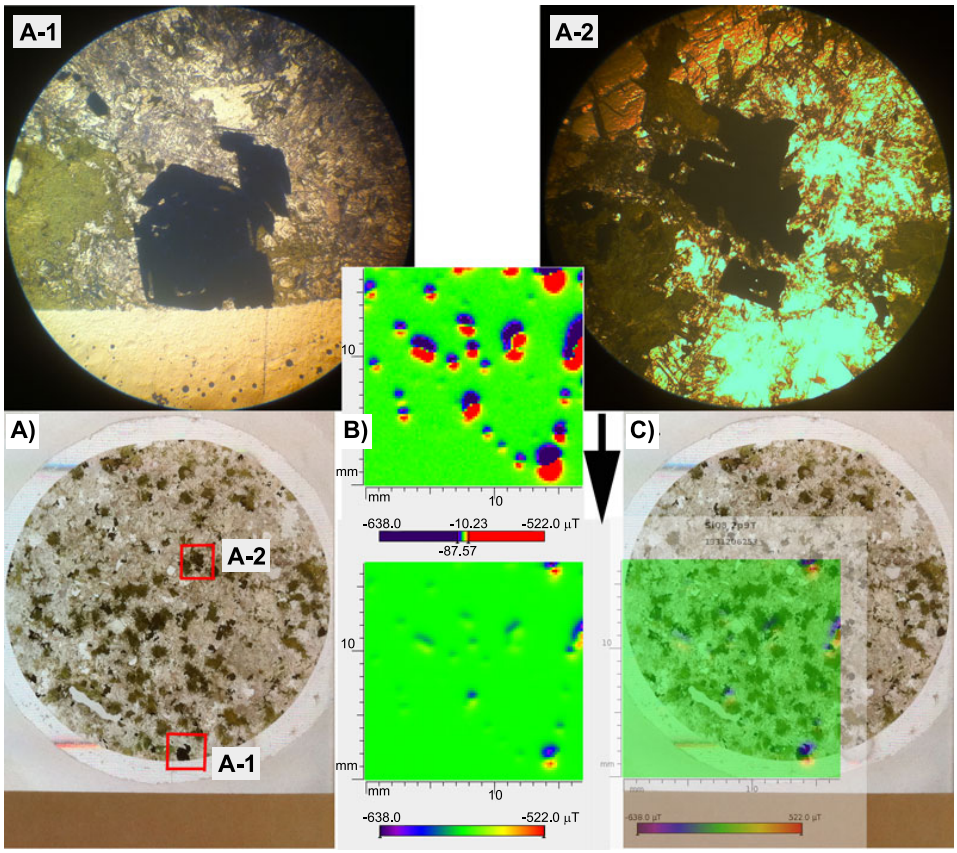

Fig. 3. Combination of the optical transparent image with the magnetic scan. **A)** Optical image of the thin section Si08. Red rectangles show the locations of the insets A-1 and A-2. **B)** Magnetic scan of Si08 pulse magnetized by 3 T along the black arrow. Top image illustrates fields from –87.57 to –10.23 µT. **C)** Overlap of the magnetic and optical images.

4. RESULTS

The magnetic image of the sample Si07 (Fig. 1B) from early Ludlow showed an eye-like magnetic texture. The image was combined with the optical image (Fig. 1C). The regions that showed significant magnetic signature of up to 22 μT (Table 1) at 0.1 mm above the surface, were looked at in more detail (red squares in Fig. 1A, A-1, A-2, using a standard polarized microscope (Spencer). The images show that these rocks contain numerous vesicles with associated amygdales. The original vesicle walls (shown in red in Fig. 1A-1) and sometimes the entire vesicle (Fig. 1A-2) is commonly filled with iron oxides. The rest of the section shows a glassy matrix and devitrified plagioclases with no significant magnetic signal. The thin section was magnetized by a pulse field in the direction parallel to the thin section, from top to bottom of the image in Fig. 1B. The magnetic map suggests that field lines are escaping from the plane of the thin section at locations of the iron oxide filled vesicle A-2 and therefore forming a dipole that is oriented in reversed direction. Magnetic structure near the partially filled vesicle A-1 is more complicated due to interaction with nearby magnetic anomalies and presence of diamagnetic material in the center of the vesicle.

Basaltic section C5 (Fig. 2) from the Wenlock (Černidla) showed a somewhat anisotropic magnetic texture with several of magnetic anomalies trending diagonally at 45° from bottom left to top right across the image (Fig. 2B). This section contained a fracture that followed the anisotropic character. Part of this texture might be created by a fracture filled with nonmagnetic (diamagnetic) minerals. Because this section is magnetized parallel to the thin section, the magnetic field lines leak to the surface at the gap. Similar magnetic structure was shown by (*Weiss et al., 2007b*). The detail of the regions near the fracture and within the matrix associated with magnetic anomalies was marked by red rectangle in Fig. 2A and shown by two insets (A-1, and A-2) where one shows the detail near the fracture and one the pyroxene grain with associated magnetic anomaly up to 61 μT for this scan. The magnetic and transmitted images were combined into one in Fig. 2C in order to localize the minerals, on the thin section, that produce the observed magnetic anomalies. This sample has clear-cut paleomagnetic characteristic and shows only little signs of either diagenetic and/or viscous overprint of the fairly stable Silurian paleomagnetic direction ($D = 227°$, $I = -26°$ or $D = 217°$, $I = -9°$ before the tilt correction) for the Prague Synform.

Table 1. Basic rockmagnetic properties.

Sample	Magnetic Susceptibility [10^{-3} SI]	NRM [A/m]	SIRM [A/m]	Magnetic Anomaly [μT]	Mean Destructive Field [mT]	Medium Magnetizing Field [mT]	Mean Destructive Field after IRM Saturation [mT]
Si07-02A	29.8	0.815	580	22	15	70	15
C5A	46.8	15.470	980	61	20	30	9
Si08-03A	9.9	0.159	320	60	10	50	15

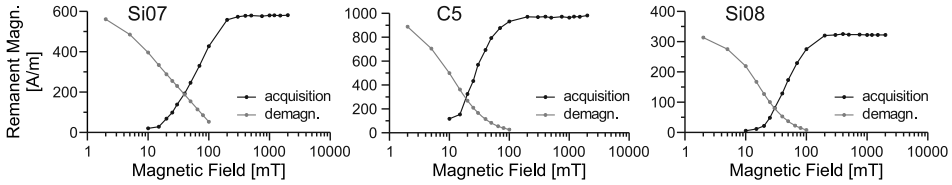

Fig. 4. Acquisition of saturation remanence and its demagnetization for samples Si07, C5, and Si08.

The Llandovery basaltic sample Si08 revealed an image with discrete magnetic anomalies separated from each other (Fig. 3B). These magnetic anomalies were almost two orders of magnitude stronger than in the previous sections and reached 1160 μT at 0.1 mm over the surface (compared with 22 μT and 61 μT for Si07 and C5, respectively, see Table 1). Optical images revealed the presence of discrete magnetic oxides up to 1 mm in size, contributing to the large magnetic signature. These oxides have sharp edges indicating that the magnetic mineral was growing in size during the solidification of the basalt.

The magnetic acquisition and demagnetization of these basalts (Fig. 4) showed that saturated state of the basaltic sample C5 was the most magnetic reaching very high saturation isothermal remanent magnetization (*SIRM*) of 980 A/m, followed by Si07 with 580 A/m and Si08 with 320 A/m (Table 1). Thus sample Si08 has the lowest overall magnetization when measured using a spinner magnetometer, however when scanned with the magscan it shows the largest magnetic anomalies.

Sample C5 had 9 mT and 30 mT values for median destructive field after IRM saturation and magnetizing field, respectively (Table 1). This is a minimum set of required fields to demagnetize or magnetize when compared with 15 mT and 70 mT medium fields for Si07 and 15 mT and 50 mT medium fields for Si08 (Table 1). Thus magnetically, sample Si07 is the hardest and sample C5 the softest.

When treating the original natural magnetic remanence (*NRM*) of these basalts (Figs 5–7), we have sample C5 with the largest remanence (15.5 A/m) followed by Si07 (0.82 A/m) and Si08 (0.16 A/m). Magnetically the sample C5 had the largest (most stable remanence) mean destructive field (*MDF*) just over 20 mT followed by almost exactly 15 mT for MDF of Si07 and magnetically weakest MDF of 10 mT was for sample Si08 (Table 1). Both C5 and Si07 show fairly stable paleodirections. Paleodirections for Si08 (Fig. 7), however, are somewhat chaotic showing a viscous overprint (this can be multidomain (MD) magnetic grains who's remanence is soft in general).

Fig. 5. (Facing page) Demagnetization of the natural remanent magnetization (*NRM*) of sample Si07. **A)** Stereonet projection, Zijderveld projection, magnetization magnitude and magnetic susceptibility plots of thermal demagnetization. **B)** Stereonet projection, Zijderveld projection, magnetization magnitude of demagnetization by alternating field.

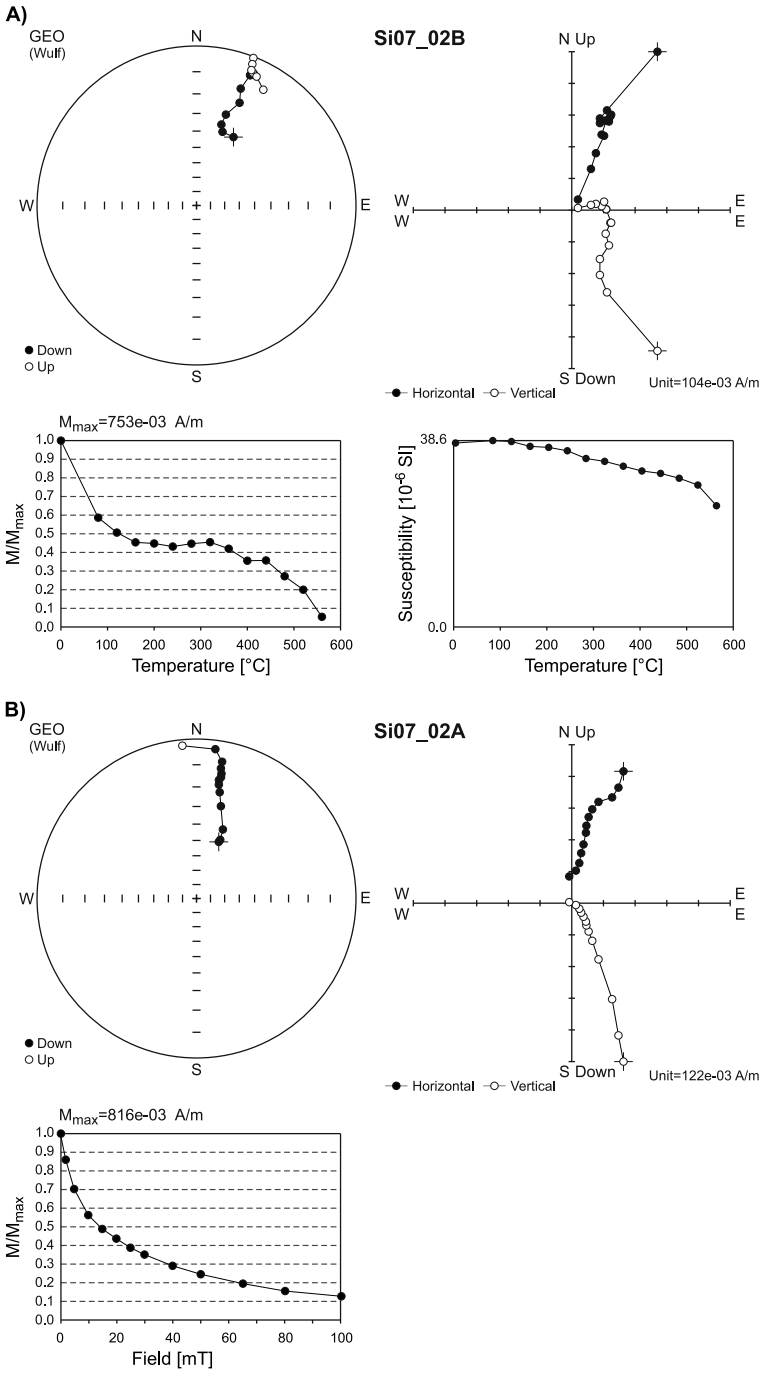
A)
GEO
(Wulf)
N
W
E
S
Down
Up
Si07_02B
N Up
W
E
W
E
S Down
Horizontal
Vertical
Unit=104e-03 A/m
M_{max}=753e-03 A/m
M/M_{max}
Temperature [°C]
38.6
Susceptibility [10^{-6} SI]
0.0
B)
GEO
(Wulf)
Si07_02A
N Up
S Down
Horizontal
Vertical
Unit=122e-03 A/m
M_{max}=816e-03 A/m
Field [mT]

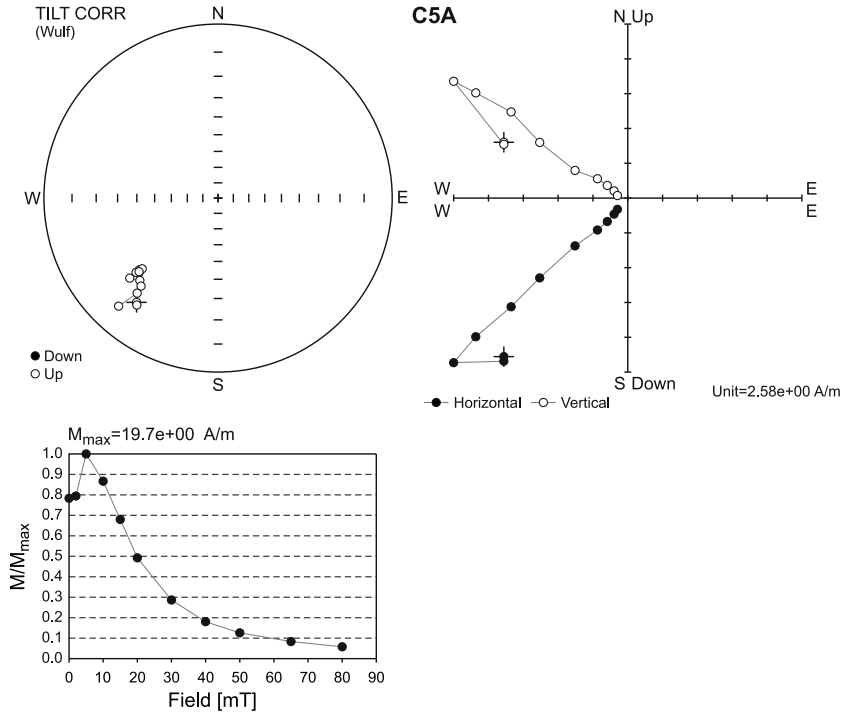

Fig. 6. Demagnetization of the natural remanent magnetization (*NRM*) of sample C5. Stereonet projection, Zijderveld projection magnetization magnitude of demagnetization by alternating field.

Thermally most stable is the sample Si07 holding medium thermal stability (MTS), 50% of its remanence, up to 300°C followed by MTS of 260°C for sample Si08. In both cases the sample starts to have slight chemical changes as revealed by the susceptibility plots (Figs 5A, 7A, lower right section). Sample Si07 shows at least three components during the thermal demagnetization while S08 at least two directional components. We did not perform the thermal demagnetization for sample C5.

5. DISCUSSION

Without magnetic maps produced by magnetic scanner the demagnetization of the remanence would be quite complicated. There are several pole directions and it is difficult to figure out which is the primary and which is the secondary component of magnetization. Even harder is to assign a specific time to individual components. However magnetic maps (Figs 1–3) helped to localize the magnetic minerals by detecting their saturation isothermal remanence imparted by 3 T pulse magnetic field parallel to the rocks' thin sections. In general saturation remanence is about two orders of magnitude larger that natural remanence (*NRM*) that carries the paleomagnetic information (*Wasilewski et al., 2002*).

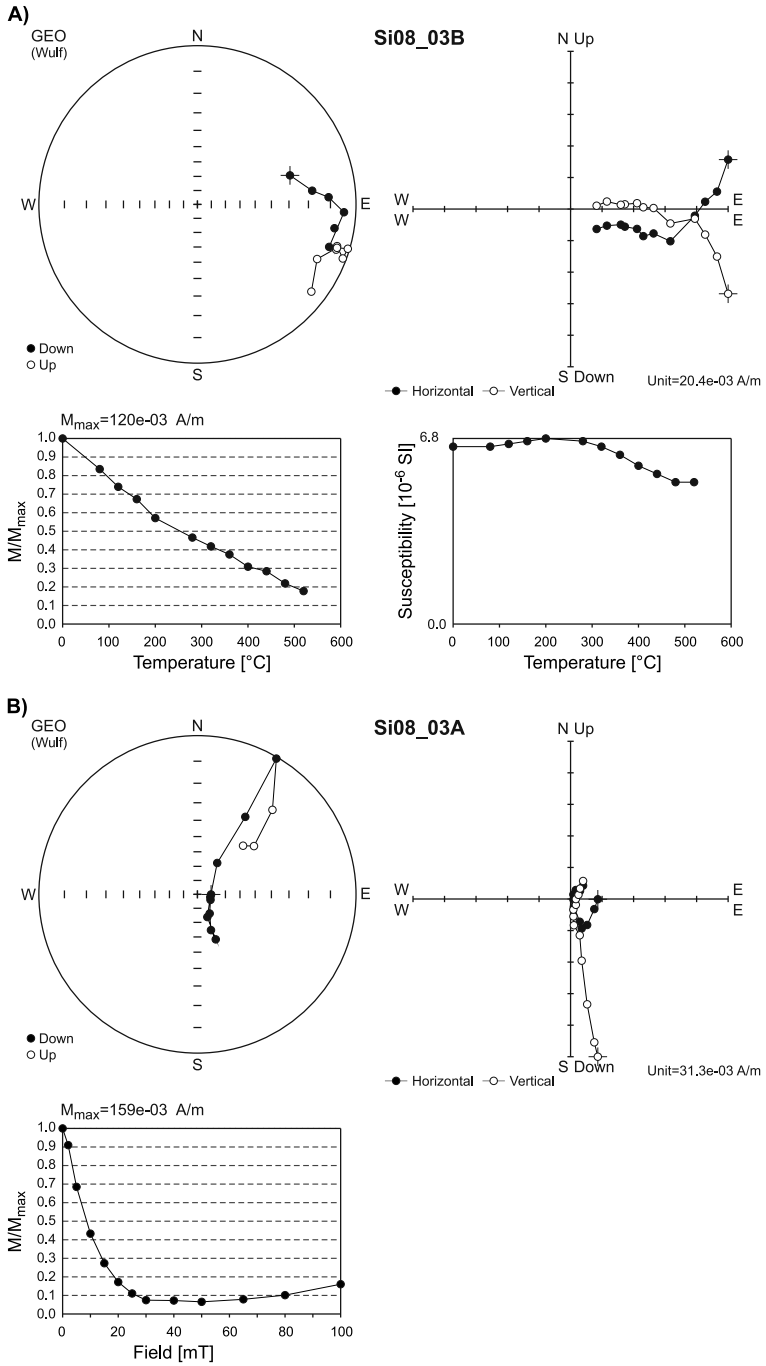

Fig. 7. The same as in Fig. 5, but for sample Si08.

For example most of the magnetic signature associated with the basalt Si07 is carried by amygdales, the secondary (diagenetic) mineralization filling the vesicles of the buried lava flow (Figs 1A, A-1, A-2). Most of the time formation of amygdales is associated with hydrothermal fluids that flow through the pores of the lava flow, dissolving the Si and Fe ions when fluids are of reduced nature and precipitating them as oxides when mixing with air inside the vesicles. The timing of this event is tied with the Permocarboniferous paleodirection (*Krs et al., 2001*) that seems to be fairly stable as shown both in AF and thermal demagnetization plots (Fig. 5). Thus hydrothermal fluids action is inferred to have occurred shortly after formation of the basalt flow, and persisted until Permocarboniferous Variscan orogeny.

The basalt characterized by sample Si08 (Fig. 3) revealed a unique characteristic of separated dipoles buried in the thin section as discrete magnetic grains whose magnitude is astounding, almost 2 orders of magnitude stronger compared with the other basaltic sections. We don't see any magnetic scaling like this in the remanence (*NRM*) characteristics. In fact the remanence of this sample is the weakest of all (0.16 A/m for Si08 compared to 0.82 A/m for Si07 and 15.5 A/m for C5, Table 1). Magnetic remanence of this basalt is somewhat chaotic and reflects the potential to acquire viscous magnetic signature by the large discrete grains in this basalt flow. Therefore, nearby magnetic disturbance would likely change the magnetic direction of individual grains according to values of individual grain magnetic coercivity. This is reflected in demagnetization plots. Thermal demagnetization at moderate temperatures looses signal of smaller magnetic carriers with lower blocking temperature while AF demagnetization at low fields looses signal of larger grains with lower magnetic coercivity. Therefore the final paleodirections differ when using either demagnetization technique. This difference, in fact, points to a unique lava flow because in principle it is possible to separate the magnetic anomalies based on the magnetic scanning according to their sizes. Smaller sizes of magnetic anomalies point to smaller magnetic volumes that have higher coercivity. Therefore, if the Prague Synform has been moving in respect to geomagnetic field, the grain size distribution of the carriers as detected in Fig. 3 would randomize the paleo directions of individual grains in such a way that it would randomize the overall magnetic signature. This is consistent with our observation that the sample Si08 has the weakest natural remanent magnetization.

From the stability point of view and paleodirection characteristics, basalt C5 appears to be most reliable. C5 does not contain amygdales or discrete soft magnetic grains. Based on Fig. 2, it suggests certain anisotropy of magnetic anomalies detected over the surface, even if we neglect the magnetic field lines escaping from the fracture in the thin section. This is likely a signature of the solidification of this specific lava flow and this give certain credibility that the magnetic signature is genuine from the time of lava flow cooling. Anisotropy of magnetic susceptibility (AMS) measurements of an adjacent rock sample has consistent direction of maximum susceptibility pointing towards north east. However, this was bulk measurement of AMS which has different physical meaning than magnetic map of the vertical component of the magnetic field lines escaping from the rock thin section. Sample C5 shows only slight signs of either viscous or diagenetic overprint (Fig. 6) that was possible to clean using 5 mT AF field.

6. CONCLUSIONS

Magnetic eye-like texture found during the scanning reveals dominant magnetic carriers associated primarily with the amygdales formed inside the lava flow's vesicles of sample Si07. Paleodirections are stable ($D = 20°$, $I = –4°$) and points to the Permocarboniferous episode during which the magnetic information from amygdales originated.

Magnetic texture of the sample Si08 revealed strongly isolated dipolar signature, therefore the sample with large distribution of grain sizes of magnetic carriers. This phenomenon, when occurring within the rock sample Si08, results in chaotic paleodirections due to variable viscosity of contrasting grain sizes of magnetic minerals. The result is overall demagnetization of the original remanence and strong viscous overprint.

Magnetic scanning of sample C5 revealed homogeneous magnetic signature with signs of anisotropy, possibly pointing to the settling of the lava flow. This sample indicates the most reliable paleomagnetic characteristic and shows only little signs of either diagenetic and/or viscous overprint of the fairly stable Silurian paleomagnetic direction ($D = 227°$, $I = –26°$ or $D = 217°$, $I = –9°$ before the tilt correction) for the Prague Synform.

Magnetic scanner proved to be a vital tool when interpreting the paleomagnetic information from the basaltic lava flows.

Acknowledgement: We want to thank Mark J. Dekkers, Mike Fuller and one anonymous reviewer for improving this paper with their review. This research is supported by the Czech Science Foundation under grant - P210/10/2351. Allen Lunsford helped with the final setup of the magnetic scanning instrument. We thank Youngwood Science and Engineering (youngwoodscience@gmail.com) for providing the MagScan software free of charge. We acknowledge help from S. Šlechta, D. Venhodová, J. Petráček, O. Man, J. Drahotová, J. Jabůrková, P. Štorch, V. Janoušek, J. Frýda and J. Trubač.

References

Acuna M.H., Anderson B.J., Russell C.T., Wasilewski P., Kletetschka G., Zanetti L. and Omidi N., 2002. NEAR magnetic field observations at 433 Eros: First measurements from the surface of an asteroid. *Icarus*, **155**, 220–228.

Aifa T., Pruner P., Chadima M. and Štorch P., 2007. Structural evolution of the Prague synform (Czech Republic) during Silurian times: An AMS, rock magnetism, and paleomagnetic study of the Svaty Jan pod Skalou dikes. Consequences for the nappes emplacement. *Geol. Soc. Amer. Spec. Pep.*, **423**, 249–265.

Bouček B., 1942. O novém odkryvu siluru u Loděnic (On new Silurian outcrop at Loděnice). *Zpravodaj Geologického Ústavu Ćechy Morava*, **17**, 165–172 (in Czech).

Chadima M. and Hrouda F., 2006. Remasoft 3.0 - a user friendly paleomagnetic data browser and analyser. *Travaux Geophysiques*, **XXVII**, 20–21.

Connerney J.E.P., Acuna M.H., Ness N.F., Kletetschka G., Mitchell D.L., Lin R.P. and Reme H., 2005. Tectonic implications of Mars crustal magnetism. *Proc. Natl. Acad. Sci. U. S. A.*, **102**, 14970–14975.

Connerney J.E.P., Acuna M.H., Wasilewski P.J., Kletetschka G., Ness N.F., Reme H., Lin R.P. and Mitchell D.L., 2001. The global magnetic field of Mars and implications for crustal evolution. *Geophys. Res. Lett.*, **28**, 4015–4018.

Fišera F., 1965a. Defilé na levém břehu Berounky mezi Lišticemi a samotou "U Vitáčka" (Defile on left bank of Berounka river between Lištice and solitude "U Vitáčka"). In: *Paleovulkanity Českého masivu (Paleovulcanites of the Bohemian Massif)*. Charles University, Prague, Czech Republic, 71–76 (in Czech).

Fišera, F., 1965b. Lom u silnice jižně od Lištic (Quarry at road south from Lištice). In: *Paleovulkanity Českého masivu (Paleovulcanites of the Bohemian Massif)*. Charles University, Prague, Czech Republic, 67–70 (in Czech).

Horný R., 1965. Tektonická stavba a vývoj siluru mezi Berounem a Tachlovicemi (Tectonic structure and development of Silur between Beroun and Tachlovice). *Časopis pro mineralogii a geologii*, **X**, 147–155 (in Czech).

Jelínek V., 1966. A high sensitivity spinner magnetometer. *Stud. Geophys. Geod.*, **10**, 58–78.

Jelínek V., 1973. Precision AC bridge set for measuring magnetic susceptibility of rocks and its anisotropy. *Stud. Geophys. Geod.*, **17**, 36–48.

Kirschvink J.L., 1980. The least-squares line and plane and the analysis of paleomagnetic data. *Geophys. J. Roy. Astron. Soc.*, **62**, 699–718.

Kletetschka G., 2000. Intense remanence of hematite-ilmenite solid solution. *Geol. Carpath.*, **51**, 187–187.

Kletetschka G., Connerney J.E.P., Ness N.F. and Acuna M.H., 2004. Pressure effects on martian crustal magnetization near large impact basins. *Meteorit. Planet. Sci.*, **39**, 1839–1848.

Kletetschka G., Fuller M.D., Kohout T., Wasilewski P.J., Herrero-Bervera E., Ness N.F. and Acuna M.H., 2006. TRM in low magnetic fields: a minimum field that can be recorded by large multidomain grains. *Phys. Earth Planet. Inter.*, **154**, 290–298.

Kletetschka G., Kohout T. and Wasilewski P.J., 2003. Magnetic remanence in the Murchison meteorite. *Meteorit. Planet. Sci.*, **38**, 399–405.

Kletetschka G., Lillis R.J., Ness N.F., Acuna M.H., Connerney J.E.P. and Wasilewski P.J., 2009. Magnetic zones of Mars: Deformation-controlled origin of magnetic anomalies. *Meteorit. Planet. Sci.*, **44**, 131–140.

Kletetschka G., Ness N.F., Connerney J.E.P., Acuna M.H. and Wasilewski P.J., 2005. Grain size dependent potential for self generation of magnetic anomalies on Mars via thermoremanent magnetic acquisition and magnetic interaction of hematite and magnetite. *Phys. Earth Planet Inter.*, **148**, 149–156.

Kletetschka G. and Stout J.H., 1998. The origin of magnetic anomalies in lower crustal rocks, Labrador. *Geophys. Res. Lett.*, **25**, 199–202.

Kletetschka G., Wasilewski P.J. and Taylor P.T., 2000a. Hematite vs. magnetite as the signature for planetary magnetic anomalies? *Phys. Earth Planet. Inter.*, **119**, 259–267.

Kletetschka G., Wasilewski P.J. and Taylor P.T., 2000b. Mineralogy of the sources for magnetic anomalies on Mars. *Meteorit. Planet. Sci.*, **35**, 895–899.

Kodym O., Bouček B. and Šulc J., 1931. *Průvodce ke geologické exkursi do okolí Berouna, Koněprus a Budňan (Guide to the Geological Excursion to the Neighbourhood of Beroun, Koněprusy and Budňany).* Czech Geological Survey, Prague, Czech Republic (in Czech).

Kříž J., 1991. The Silurian of the Prague Basin - tectonic, eustatic and volcanic controls on facies and faunal development. In: Bassett M.G., Lane O.D. and Edwards D. (Eds.), *The Murchison Symposium: Proceedings of an International Conference on the Silurian System.* Special Papers in Palaeontology 44, Palaeontological Association, London, U.K, 179–203.

Kříž J., 1992. *Silurian Field Excursion, Prague Basin (Barrandian), Bohemia.* National Museum of Wales Geol. Ser. 13, 111 pp.

Kříž J., 1998. Silurian. In: Chlupáč I., Havlíček V., Kříž J., Kukal Z. and Štorch P. (Eds.), *Paleozoic of Barrandian (Cambrian to Devonian)*. Czech Geological Survey, Prague, Czech Republic, 79–100.

Krs M., Pruner P. and Man O., 2001. Tectonic and paleogeographic interpretation of the paleomagnetism of Variscan and pre-Variscan formations of the Bohemian Massif, with special reference to the Barrandian terrane. *Tectonophysics*, **332**, 93–114.

Man O., 2003. Analysis of multi-component natural remanent magnetization based on the thermal demagnetisation spectrum. *Stud. Geophys. Geod.*, **47**, 359–370.

Oda H., Usui A., Miyagi I., Joshima M., Weiss B.P., Shantz C., Fong L.E., McBride K.K., Harder R. and Baudenbacher F.J., 2011. Ultrafine-scale magnetostratigraphy of marine ferromanganese crust. *Geology*, **39**, 227–230.

Příhoda K., Krs M., Pešina B. and Bláha J., 1989. MAVACS-A new system of creating a nonmagnetic environment for paleomagnetic studies. *Cuadernos de Geologica Ibérica*, **12**, 223–250.

Strnad J., 1961. Datolitové rohovce-surovina boru (Datolite chert materials). *Časopis pro mineralogii a geologii*, **IV**, 157–160 (in Czech).

Uehara M., van der Beek C.J., Gattacceca J., Skidanov V.A. and Quesnel Y., 2010. Advances in magneto-optical imaging applied to rock magnetism and paleomagnetism. *Geochem. Geophys. Geosyst.*, **11**, Q05Y09, DOI: 10.1029/2009GC002653.

Wasilewski P., Acuna M.H. and Kletetschka G., 2002. 433 Eros: Problems with the meteorite magnetism record in attempting an asteroid match. *Meteorit. Planet. Sci.*, **37**, 937–950.

Weiss B.P., Kirschvink J.L., Baudenbacher F.J., Vali H., Peters N.T., Macdonald F.A. and Wikswo J.P., 2000. A low temperature transfer of ALH84001 from Mars to Earth. *Science*, **290**, 791–795.

Weiss B.P., Lima E.A., Fong L.E. and Baudenbacher F.J., 2007a. Paleointensity of the Earth's magnetic field using SQUID microscopy. *Earth Planet. Sci. Lett.*, **264**, 61–71.

Weiss B.P., Lima E.A., Fong L.E. and Baudenbacher F.J., 2007b. Paleomagnetic analysis using SQUID microscopy. *J. Geophys. Res.*, **112**, B09105, DOI: 10.1029/2007JB004940.